Archives of Biochemistry and Biophysics 506 (2011) 142–149

Contents lists available at ScienceDirect

Archives of Biochemistry and Biophysics

journal homepage: www.elsevier.com/locate/yabbi

Hydrophobic amino acids at the cytoplasmic ends of helices 3 and 6 of rhodopsin conjointly modulate transducin activation

Laia Bosch-Presegué [a,1], Laura Iarriccio [a], Mònica Aguilà [a], Darwin Toledo [a], Eva Ramon [a], Arnau Cordomí [b], Pere Garriga [a,*]

[a] Centre de Biotecnologia Molecular, Departament d'Enginyeria Química, Universitat Politècnica de Catalunya, 08222 Terrassa, Spain
[b] Laboratori de Medicina Computacional, Unitat de Bioestadística, Facultat de Medicina, Universitat Autònoma de Barcelona, 08193 Cerdanyola del Vallès, Spain

ARTICLE INFO

Article history:
Received 10 October 2010
and in revised form 22 November 2010
Available online 27 November 2010

Keywords:
G-protein-coupled receptor
Rhodopsin
Muscarinic receptor
G-protein activation
Visual phototransduction

ABSTRACT

Rhodopsin is the visual photoreceptor responsible for dim light vision. This receptor is located in the rod cell of the retina and is a prototypical member of the G-protein-coupled receptor superfamily. The structural details underlying the molecular recognition event in transducin activation by photoactivated rhodopsin are of key interest to unravel the molecular mechanism of signal transduction in the retina. We constructed and expressed rhodopsin mutants in the second and third cytoplasmic domains of rhodopsin – where the natural amino acids were substituted by the human M3 acetylcholine muscarinic receptor homologous residues – in order to determine their potential involvement in G-protein recognition. These mutants showed normal chromophore formation and a similar photobleaching behavior than WT rhodopsin, but decreased thermal stability in the dark state. The single mutant V138$^{3.53}$ and the multiple mutant containing V227$^{5.62}$ and a combination of mutations at the cytoplasmic end of transmembrane helix 6 caused a reduction in transducin activation upon rhodopsin photoactivation. Furthermore, combination of mutants at the second and third cytoplasmic domains revealed a cooperative role, and partially restored transducin activation. The results indicate that hydrophobic interactions by V138$^{3.53}$, V227$^{5.62}$, V250$^{6.33}$, V254$^{6.37}$ and I255$^{6.38}$ are critical for receptor activation and/or efficient rhodopsin–transducin interaction.

Introduction

Rhodopsin is the visual photoreceptor present in rod cells and responsible for dim light vision in the vertebrate retina [1,2]. This receptor has seven transmembrane (TM)[2] helices and is a prototypical member of the G-protein-coupled receptors (GPCRs) superfamily [3–5], being the only member whose structure was resolved by X-ray crystallography for almost a decade [6], when other GPCRs structures were also solved [7,8]. This visual receptor has unique structural features, such as having its ligand, 11-*cis*-retinal, covalently bound through a protonated Schiff-base linkage to K296$^{7.43}$ (where the superscript indicates the consensus numbering according to Ballesteros and Weinstein [9]). Retinal isomerization, upon light absorption, induces structural changes in the helical bundle that are transmitted to the cytoplasmic domain where the interaction with transducin (Gt) occurs. Upon physical binding to rhodopsin, Gt is activated and initiates the visual phototransduction cascade. Structural and functional studies on rhodopsin, and other GPCRs, provide clues about common key sequence motifs in this family of receptors and allow elucidating the molecular bases of the activation mechanism [10,11].

Muscarinic receptors are prototypical class I GPCRs – belonging to the same subfamily as rhodopsin – and are located in the parasympathic nervous system. The study of muscarinic receptors is of outstanding pharmacological interest because they have been involved in a wide variety of physiological and pathophysiological processes like Alzheimer and Parkinson [12,13]. Muscarinic receptors have an orthosteric site for its native ligand acetylcholine within the TM region. The binding of agonists promotes receptor activation through specific conformational changes that are ultimately transmitted to the intracellular domain. The newly adopted conformation of the TM helices, and cytoplasmic loops presenting its recognition sites, facilitates G protein binding and activation [14,15]. There are 5 muscarinic receptor subtypes differentially expressed and associated with various types of G proteins and second messenger systems [15–20]. M3 muscarinic receptor is preferentially coupled to the G_q family [21].

The knowledge of the structural details accompanying the transition between the inactive to the active states of GPCRs and the

* Corresponding author. Fax: +34 937398225.
E-mail address: pere.garriga@upc.edu (P. Garriga).
[1] Present address: Chromatin Biology Laboratory, Cancer Epigenetics and Biology Program (PEBC) IDIBELL, Barcelona, Catalonia, Spain.
[2] *Abbreviations used:* A, absorbance; GPCRs, G-protein-coupled receptor; Gt, transducin; GtαCt, C-terminal end of Gt α subunit; Metal, Metarhodopsin I; MetaII, Metarhodopsin II; TM, transmembrane; WT, wild type.

0003-9861/$ - see front matter © 2010 Elsevier Inc. All rights reserved.
doi:10.1016/j.abb.2010.11.019

subsequent transduction to signaling proteins has increased dramatically in the last years. In the case of rhodopsin, different studies showed two binding clefts in Gt for activated rhodopsin: one in the C-terminal region of the α subunit (GtαCt) and the other in the farnesylated C-terminal end of the γ subunit [22–25]. Early mutagenesis studies proposed that GtαCt was recognized by the second and third cytoplasmic domains, and specifically by residues Y136$^{3.51}$, V137$^{3.52}$, V138$^{3.53}$, V139$^{3.54}$, E247$^{6.32}$, L248$^{6.31}$, E249$^{6.32}$, V250$^{6.33}$ and T251$^{6.34}$ [26]. The release of two ligand-free opsin crystal structures that contain features of the putative active states [27,28], and in particular the structure of opsin in its G-protein-interacting conformation, paved the way towards a better understanding of the specific roles of each specific residue with regard to G-protein activation and signal transmission. The structures confirmed the outward movement of the cytoplasmic end of TM6 [29] relative to the TM core that was known to occur upon Metarhodopsin II (MetaII) formation. This movement, a conserved feature of this family of receptors [30], allows that residues involved in Gt activation become exposed [31–33]. GtαCt has been proposed to interact with residues in the C-terminal end of TM6, exposed as a result of the helical movement. In particular, it has been hypothesized that hydrophobic contacts would control Gt–rhodopsin affinity interaction [34]. V250 would be involved in the slight rotation of TM6 in Metarhodopsin I (MetaI) and subsequent transfer to a more hydrophobic environment, in the interface between TM3 and TM5, upon further movement of TM6. V227$^{5.62}$ was also found to be involved in the movement of TM5 in MetaI triggered by the ring of the isomerized retinal. This movement in TM5 would precede the larger scale movement of TM6 in MetaII [35].

It is well known that the cytoplasmic segments of GPCRs, particularly the second and the third cytoplasmic domains – including the loops and adjacent helix ends, and to some extent the C-terminal tail of the receptor –, play a critical role in the interaction with G-proteins and in the molecular mechanism of subsequent activation and signaling. Different studies allowed the identification of rhodopsin–Gt interacting sites [28,36,37] as well as the M3 muscarinic domains involved in G_q recognition [37–41]. The second and third cytoplasmic domains and proximal membrane region of the C-terminus are important in this G_q recognition. These studies showed that Y5.62, in the rat M3 receptor, is essential for G_q activation. This residue is conserved in M1, M3 and M5 receptors, which signal via G_q, whereas M2 and M4 receptors, signaling via $G_{i/o}$, exhibit Ser at the equivalent position. It was hypothesized that Y5.62 amino acid could form, together with A6.33, A6.34, L6.37 and S6.38, a site for G_q recognition [39]. Additionally, it was described that the introduction of C-II loop M3 in a M2 receptor background increased phosphoinositol hydrolysis. In particular, four amino acid residues of C-II M3 muscarinic loop, S168$^{3.53}$, R171$^{3.56}$, R176$^{C\text{-}II}$ and R183$^{C\text{-}II}$, were found to be critical for G_q specificity [39]. A recent study showed that it was possible to modulate G-protein selectivity by engineering the cytoplasmic domains of the membrane receptor [42]. In particular, photoactivation of rhodopsin–β_2-adrenergic chimeric receptors made on a rhodopsin construct containing the cytoplasmic domains of the β_2-adrenergic receptor resulted in cAMP synthesis, supporting the hypothesis of a possible common mechanism for all Class I GPCRs. In the present study we have used an analogous approach using the rhodopsin sequence as the main core and replacing amino acids at the second and third cytoplasmic domains by those of the human M3 receptor, with the aim of pinpointing specific amino acids in these regions involved in the formation of defined structural domains backing G-protein recognition specificity.

Rhodopsin/M3 mutants showed chromophore formation and photobleaching behavior similar to wild-type (WT) rhodopsin. The hydroxylamine reactivity was not affected suggesting that the mutants had a dark conformation similar to the WT receptor. V138S$^{3.53}$, 4CIII$^{6.33\text{-}38}$, 5CIII$^{5.62/6.33\text{-}38}$, 1CII-5CIII and 2CII-5CIII mutants (Table 1) showed a significant reduction in Gt activation. Interestingly, mutations at the cytoplasmic end of helix 6 partially restored the Gt activation capability of the receptor suggesting a coupling of the second and third cytoplasmic loops in rhodopsin–Gt optimal interaction. The results provide experimental evidence that residues V138$^{3.53}$, V227$^{5.62}$, V250$^{6.33}$, V254$^{6.37}$ and I255$^{6.38}$ located in the TMs segments adjacent to C-II and C-III rhodopsin loops participate in receptor activation and/or Gt binding. The hydrophobic interactions involving these residues would be an important factor mediating rhodopsin–Gt interaction. Furthermore, based on Gt activation recovery of combined mutants, a conjoined action of TM3 and TM6 helices studied is proposed.

Materials and methods

Materials

11-*cis*-retinal was a gift of Prof. P.P. Philippov (Moscow State University, Russia) and Prof. A.R. de Lera (University of Vigo, Spain). Purified mAb rho-1D4 was obtained from the National Culture Center, Minneapolis and was coupled to CNBr-activated Sepharose 4 Fast Flow (Amersham Pharmacia Biotech). *n*-Dodecyl-β-D-maltoside (dodecyl maltoside, DM) was purchased from Anatrace. COS-1 cells (ATCC No. CRL-1650) were from American Type Culture Collection (Manassas, VA). Complete™ protease inhibitor mixture was from Roche Molecular Biochemicals and was used at a concentration of 1 tablet/75 ml of buffer. Purified Gi/qα subunit chimera was supplied by Calbiochem.

Construction of opsin mutants

Mutations were introduced into the synthetic bovine opsin gene by site directed mutagenesis on the WT sequence [43]. The correct sequence of the mutations introduced was confirmed by DNA sequencing using the dideoxy chain-terminated method. Rhodopsin mutants studied are shown in Table 1.

Expression and purification of WT and mutant rhodopsins

WT and mutant opsin genes were expressed in transiently transfected monkey kidney cells (COS-1) as described [44]. After the addition of 30 μM 11-*cis*-retinal in the dark, the transfected COS-1 cells were solubilized in 1% DM, and the proteins were purified by immunoaffinity chromatography using the Rho-1D4 monoclonal antibody [45]. Rhodopsins were eluted in 2 mM Na_2HPO_4,

Table 1
Rhodopsin–M3 muscarinic mutants used in this study. The rhodopsin–M3 muscarinic mutants listed here were designed, constructed, expressed and characterized as described under Materials and Methods. We also studied the stability of both inactive and active states of the mutant receptors. The mutations are located on the second cytoplasmic loop (C-II), the third cytoplasmic loop (C-III) and combinations of C-II and C-III mutations (C-II/C-III). The abbreviation system used to name the rhodopsin–M3 muscarinic mutants is original residue – amino acid number in the rhodopsin sequence – mutated residue (single point mutants); and number of mutations - loop where the mutations are located, either CII or CIII (multiple mutants).

Mutant	Location	Abbreviation
V138S	C-II	V138S
K141R	C-II	K141R
H152R	C-II	H152R
V138S/K141R/H152R	C-II	3CII
V227Y	C-III	V227Y
V250A/T251A/V254L/I255S	C-III	4CIII
V227Y/V250A/T251A/V254L/I255S	C-III	5CIII
V138S/V227Y/V250A/T251A/V254L/I255S	C-II/C-III	1CII-5CIII
V138S/K141R/V227Y/V250A/T251A/V254L/I255S	C-II/C-III	2CII-5CIII

pH 6, 0.05% DM and the completely folded fractions of these mutants were the ones used in this study.

UV–visible absorption spectra of WT and C-II, C-III and C-II/C-III mutant rhodopsins

Spectra were performed at 20 °C with a Varian Cary 100Bio spectrophotometer equipped with water-jacketed cuvette holders connected to a circulating water bath. All spectra were recorded with a bandwidth of 2 nm. For photobleaching experiments samples were illuminated with a 150-watt fiber optic light equipped with a >495-nm long-pass filter for 10 s, and the corresponding bleached spectrum were recorded immediately after illumination. Acidification of the samples was carried out with 10 µl 1 N HCl (1/10 dilution).

Thermal stability in the dark and hydroxylamine reactivity for WT and rhodopsin mutants

Rhodopsin thermal stability in the dark was followed by monitoring the loss of the maximum absorbance band in the visible region (A_{500nm}) as a function of time, at a constant temperature (55 °C). Scans were collected every 5 min and data were normalized and fit to single exponential functions using SigmaPlot to derive the $t_{1/2}$ values. Here, thermal stability stands for the stability of the chromophore covalently linked to the opsin apoprotein in the binding pocket. The overall thermal stability of the protein should be determined by other approaches. In any case, our experiments provide an indirect measurement of the degree of conformational similarity for dark structures of the rhodopsin mutants in comparison to the WT receptor. Hydroxylamine treatment was performed by adding this reagent (pH 7.0) to the sample to a final concentration of 30 mM at 20 °C. Hydroxylamine reactivity was determined by monitoring overtime the decrease of A_{500nm}.

Meta II stability for the C-II, C-III and C-II/C-III rhodopsin mutants

In order to determine the stability for the rhodopsin mutants active state, we monitored the stability of the Schiff Base covalent binding between the retinal and K296 [46]. To do that, rhodopsin samples purified in 2 mM Na_2HPO_4, pH 6, 0.05% DM were illuminated for 10 s and acidified with 1% 2 N H_2SO_4 at different intervals of time. A_{440nm}, corresponding to the remaining Schiff-base linkage [47], was recorded overtime, plotted, and $t_{1/2}$ values were determined from the curves and compared to that for WT rhodopsin.

G-protein activation assay

Gt activation levels were determined by measuring the binding of radioactive GTPγ^{35}S to Gt molecules induced by WT and mutant rhodopsins as described previously [48,49]. Briefly, the reaction mixture, containing 1 µM Gt or Gi/qα chimera, 20 nM rhodopsin, 10 mM Tris–HCl (pH 7.4), 100 mM NaCl, 5 mM $MgCl_2$, 2 mM DTT, 0.012% DM, and 3 µM GTPγ^{35}S, was bleached for 30 s by using a 150-watt power source with a 495 nm cutoff filter. Samples were incubated at room temperature for 1 h, and the reactions were stopped by the addition of 10 mM Tris–HCl (pH 7.4), 100 mM NaCl, and 10 mM EDTA. Unbound GTPγ^{35}S was removed by microfiltration. The amount of GTPγ^{35}S bound to the G-protein was determined by using a TRI-CARB 2100TR scintillation counter from Packard Instrument Co. Basal Gt activation was determined as described above but keeping samples in the dark.

Molecular modeling

The computational models of inactive rhodopsin mutants were constructed on the basis of crystal structure 1GZM [50], whereas the active models relied on the opsin structure crystallized with a peptide based on GtαCt, PDB entry: 3DQB [28]. The conformations of the mutated side-chains were selected based on a library of rotamers implemented in PyMol [51] All systems were energy minimized in bulk using the Amber99sb force field [52]. All figures were created using PyMol [51].

Results

Characterization of the C-II mutants

V138S, K141R, H152R, and triple mutant V138S/K141R/H152R (3CII) were purified in 2 mM Na_2HPO_4, pH 6 containing 0.05% DM and spectra were recorded in order to determine their final protein yield. All C-II mutants showed a lower yield, especially for the triple mutant 3CII with a fifteen-fold lower yield, when compared to WT rhodopsin (Fig. 1B, Table 2). The photobleaching and acidification behavior of the purified mutant rhodopsins were also WT-like, suggesting that these mutants underwent the same photoactivation pathway than WT rhodopsin (data not shown). In the dark, they all showed a very similar visible absorption band with a λ_{max} around 500 nm, indicating that the introduction of these mutations did not affect the retinal binding pocket configuration (Fig. 1B, Table 2). However, thermal stability in the dark state – measured at 55 °C – showed differences with regard to WT. All the single mutants showed a slightly increased stability in the dark, especially in the case of H152R. Upon combination of these single mutants in the 3CII triple mutant, the resulting receptor showed a decrease in the thermal stability. All C-II mutants showed no hydroxylamine sensitivity in the dark, reflecting a compact structure around the Schiff-base linkage (data not shown). These experiments, taken together, indicated that the mutations introduced did not cause gross structural perturbations in the rhodopsin dark structure compared to the WT. In addition, we also determined the MetaII stability of the purified mutants by means of a fluorescence spectroscopic assay which measures retinal release (Table 2). V138S mutant showed MetaII stability similar to WT, and a slight decrease was observed in H152R mutant (0.8). On the other hand, K141R mutant showed only a MetaII stability of 0.6 when compared to WT, meaning that the introduction of this mutation destabilized the active receptor conformation (values are relative to those for WT rhodopsin taken as 1.00).

Characterization and Meta II stability of C-III mutants

V227Y, V250A/T251A/V254L/I255S (4CIII), and V227Y/AALS (5CIII) mutants were expressed and immunopurified as described in the *Experimental Procedures* section. These single and multiple mutants showed similar yield and spectroscopic features to those of WT rhodopsin (Fig. 1C, Table 2) with the λ_{max} around 500 nm. These results indicate that these mutants showed a dark state and a retinal binding pocket similar to WT protein. The thermal stability (Table 2) and hydroxylamine reactivity in the dark for these mutants were also determined. None of the C-III mutants showed chemical reactivity towards hydroxylamine, indicating that the receptor structure around the Schiff-base linkage is compact for these mutants (data not shown). On the other hand, single mutant V227Y, showed a slightly decrease on the thermal stability in the dark (0.8), and a dramatic decrease was observed in both 4CIII and 5CIII mutants (around 0.2 in both cases). One of the explanations for the acute changes detected in the dark receptor

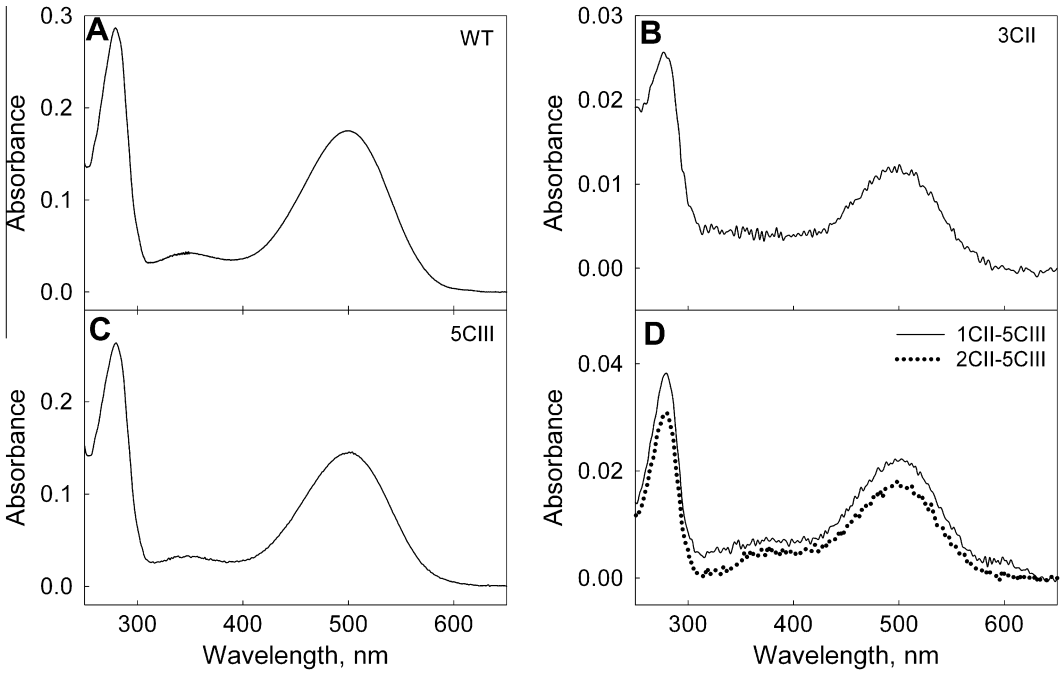

Fig. 1. UV–visible spectra for WT and 3CII, 5CIII, 1CII-5CIII and 2CII-5CIII rhodopsin mutants. WT and rhodopsin mutants were expressed into COS-1 cells and immunopurified in 2 mM Na_2HPO_4, pH 6, 0.05% DM. The spectra correspond to the correctly folded fractions, recorded at 20 °C. (A) WT rhodopsin spectra. (B) UV–Visible spectra of the C-II rhodopsin–M3 mutant, where the single mutations on the second cytoplasmic domain studied here were combined. (C) Spectra of the C-III mutants, containing the changes introduced on the third cytoplasmic domain. (D) Spectra of the C-II/C-III rhodopsin–M3 muscarinic mutants, where the mutations located at the second and third cytoplasmic domains were combined.

Table 2
UV–Visible characterization, thermal stability, MetaII Stability and Gt activation of the Rho-M3 muscarinic mutants. WT and mutant rhodopsin were expressed in COS-1 cells and immunopurified in 2 mM Na_2HPO_4, pH 6 containing 0.05% DM. Only the correctly folded fractions were used for the assays. After purification, spectra were recorded at 20 °C for each mutant and the λ_{max} was determined. Chromophore thermal stability, in the dark state, was measured by the decrease of λ_{max} overtime at 55 °C. Spectra were recorded on a spectrophotometer equipped with a water-jacketed cuvette holder connected to a circulating bath to keep stable the temperature. MetaII stability of WT and mutant rhodopsins was determined by monitoring the stability of the Schiff-base linkage between retinal and K296, upon rhodopsin illumination [46]. Briefly, WT rhodopsin and rhodopsin–M3 muscarinic mutants were illuminated for 10 s and acidified at different intervals of time with 2 N H_2SO_4. A_{440nm} was monitored overtime and values were plotted in a graph. $t_{1/2}$ were obtained from the plot. Gt activation was performed as described under Materials and Methods section. All results are normalized to the WT value taken as 1.00. All values are from three different independent rhodopsin purifications. Basal Gt activation is shown between brackets.

Rhodopsin	λ_{max} (nm)	Dark state thermal stability	MetaII stability	Gt activation
WT	500	1.00	1.00	1.00 (0.1 ± 0.05)
V138S	500	1.2 ± 0.02	1.0 ± 0.04	0.5 ± 0.07 (0.02 ± 0.16)
K141R	499	1.1 ± 0.05	0.6 ± 0.05	1.07 ± 0.07 (0.01 ± 0.11)
H152R	501	1.3 ± 0.03	0.8 ± 0.03	0.9 ± 0.1 (0.06 ± 0.02)
3CII	501	0.8 ± 0.02	N.D.[a]	1.1 ± 0.09 (0.36 ± 0.06)
V227Y	501	0.8 ± 0.03	0.8 ± 0.05	0.7 ± 0.2 (0.05 ± 0.01)
4CIII	500	0.2 ± 0.02	1.0 ± 0.04	0.3 ± 0.02 (0.03 ± 0.01)
5CIII	501	0.2 ± 0.03	1.2 ± 0.02	0.1 ± 0.05 (0.03 ± 0.02)
1CII-5CIII	501	0.5 ± 0.01	N.D.∗	0.04 ± 0.04 (0.06 ± 0.03)
2CII-5CIII	500	0.5 ± 0.01	N.D.∗	0.4 ± 0.15 (0.09 ± 0.05)

[a] N.D.: not determined.

conformation stability on these multiple mutants could be the introduction of a large number of mutations on the same protein construct. On the other side, we measured MetaII stability for these intracellular C-III mutants and we did not observe changes in active receptor conformation stability. However, we noticed that when alone, V227Y mutant showed a slightly decrease on the stability of its active conformation (0.8), whereas when combined with 4-CIII mutant, the stability increased 1.5-fold.

Characterization and MetaII stability of the C-II-C-III mutants

C-II and C-III mutants were combined with the aim to determine if these C-II and C-III amino acids formed a common site for G-protein recognition and/or activation. V138S/V227Y/V250A/T251A/V254L/I255S (1CII-5CIII) and V138S/K141R/V227Y/V250A/T251A/V254L/I255S (2CII-5CIII) combined mutants were regenerated with 11-*cis*-retinal and showed a sixfold lower protein yield, but chromophore regeneration levels similar to WT (Fig. 1D, Table 2). These mutants showed no hydroxylamine sensitivity in the dark, and their photobleaching and acidification properties were very similar to those of WT rhodopsin (data not shown). Intrinsic chromophore thermal stability of the 1CII-5CIII and 2CII-5CIII mutants was determined by monitoring the decrease of A_{500nm} values at 55 °C overtime. Both mutants showed about 50% reduction in the dark state stability similarly to what was seen for the C-II mutants (Table 2). The introduction of a large number of mutations could likely affect the receptor inactive conformation stability.

Gt activation for the C-II, C-III and C-II/C-III mutants

The Gt activation experiments were carried out with detergent-solubilized and purified rhodopsins in 2 mM Na_2HPO_4, pH 6, 0.05% DM by means of a radioactive binding assay (Fig. 2 and Table 2). After light activation, K141R, H152R mutants showed Gt activation levels comparable to WT but V138S mutant showed up to a 50% reduction in Gt activation. It was previously reported that V138, together with Y136, V137 and V139, forms a crucial cluster for Gt interaction and mutations in these amino acids were expected to significantly reduce Gt activation [26,29,53]. The level of Gt activation for the triple mutant 3CII was 1.1 (with regard to WT) indicating that the combination of V138S, K141R and H152R single mutations restores the V138S phenotype. We also analyzed basal Gt activation, i.e. Gt activation in the dark, by the purified mutants. 3CII showed a significant increase in Gt activation in the dark (0.4) with regard to the basal Gt activation for the WT (0.1) suggesting that some of these mutations can cause structural changes in the receptor resulting in a partially active receptor in the dark. In the case of the 3CII mutant, the basal activity seems to be related to the contributions of the K141R and H152R mutations. In this case, Arg introduction at C-II would cause a conformational change in this intracellular loop allowing the interaction with Gt in the dark.

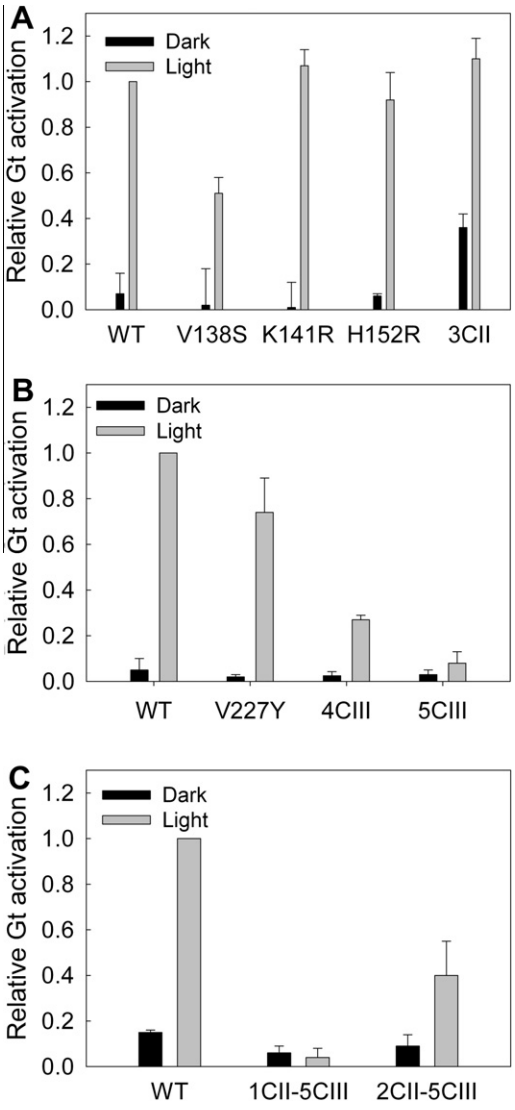

Fig. 2. Gt activation for the WT rhodopsin and the C-II, C-III, and C-II/C-III rhodopsin mutants. The activation of Gt for the single and multiple mutants studied here was determined by the incorporation of radioactive GTPγ^{35}S in Gt upon rhodopsin photoactivation. WT rhodopsin and rhodopsin–M3 muscarinic mutants were purified in 2 mM Na_2HPO_4, pH 6, 0.05% DM and mixed to a final concentration of 20 nM with 1 μM Gt in 10 mM Tris–HCl (pH 7.4), 100 mM NaCl, 5 mM $MgCl_2$, 2 mM DTT, 0.012% DM, and 3 μM GTPγ^{35}S. Upon illumination, samples were incubated at room temperature and the reaction was quenched by the addition of EDTA. Free GTPγ^{35}S was washed by filtration and the GTPγ^{35}S bound to Gt amount was measured. Data were compared to WT rhodopsin. Basal Gt activation was performed as indicated above but keeping the samples always in the dark. (A) Gt activation for the C-II rhodopsin–M3 muscarinic mutants in the dark (black) and the light (grey), (B) Gt activation upon illumination of the C-III rhodopsin–M3 muscarinic mutants, (C) Basal Gt activation (dark, in black) and after photoactivation (light, in grey) of the C-II/C-III rhodopsin–M3 muscarinic mutants.

The ability of intracellular C-III loop mutants to activate Gt was also analyzed. A reduction of about 30% on Gt activation was observed for mutant V227Y (0.7). In the case of the 4CIII mutant the maximum activation value was found to be 0.3 and for the combined 5CIII mutant, this was dramatically reduced (0.1). In the M3 muscarinic receptor, the homologous amino acids have been described to be in close contact possibly forming a common site for G protein interaction [39]. We also examined the effect of C-II and C-III conjugated mutations on Gt activation capacity. 1CII-5CIII mutant showed a maximal Gt activation value of 0.04 with regard to WT protein. The V138S single mutant showed a 50% reduction in Gt activation, and the 5CIII mutant did not show any detectable functionality. Thus, combining these mutations results in a non-functional receptor. On the other side, 2CII-5CIII mutant presented a Gt activation level of 0.4 after photoactivation. R141 K partially restored Gt activation, probably as a result of a structural change in the 1CII-5CIII mutant receptor directly affecting the rhodopsin–Gt interaction pattern. No detectable increase in the Gi/qα protein activation was detected over basal WT rhodopsin levels for any of the mutants studied (data not shown).

Modeling of the second and third cytoplasmic domains

Fig. 3, shows a model of the opsin – GtαCt complex that is in agreement with the current knowledge regarding GPCR-G protein interactions [28,37,54]. Positions mutated in the TM5–6 region (C-III domain mutations) lie close to GtαCt, whereas those at the TM3-4 segment (C-II domain mutants) exhibit contacts with either the C-terminus or the α5 helix and the adjacent β-sheet of the Gtα subunit. A more detailed localization of residues V138$^{3.53}$, K141$^{3.56}$ and H152$^{4.41}$, both in the dark-state and in the Gt-interacting conformation opsin crystal structures, is shown in Fig. 4A and B. In the inactive model, V138 flanks the ionic lock but does not participate in hydrophobic interactions with other helices, whereas in the active model, V138 interacts with L72 at the most C-terminal part of C-I, but not with the highly conserved hydrophobic residues of GtαCt. Table 3 summarizes some of the features derived from the molecular models suggesting that the close proximity to GtαCt requires a small side-chain at the 138 position. K141 forms hydrogen bond interactions with residues in the C-III loop in the inactive form and probably contacts *E342* and *N343* (Gt residues are displayed in italics for clarity) in the active state. This position contains polar/charged residues in most class I GPCRs. The model in Fig. 3 suggests that K141$^{3.56}$ could contact the α5 helix and the adjacent β-sheet of the Gtα subunit in addition to the C-terminus. H152$^{4.41}$ does not face Gt although it interacts with two aromatic residues at the C-II loop both in the inactive and in the G-protein interacting opsin structure that are close to E134$^{3.49}$. However, none of these interactions seems to be functionally important as H152R did not show any significant effect on Gt activation.

Localization of residues V227$^{5.62}$, V250$^{6.33}$, T251$^{6.34}$, V254$^{6.37}$ and I255$^{6.38}$ is shown in a corresponding molecular model (Fig. 4C and D). In the inactive state, T251 and V254 are strongly packed to TM3, V250 faces TM2 and I255 points to TM5. T251 is known to be part of the ionic-lock between TMs 3 and 6 [49],

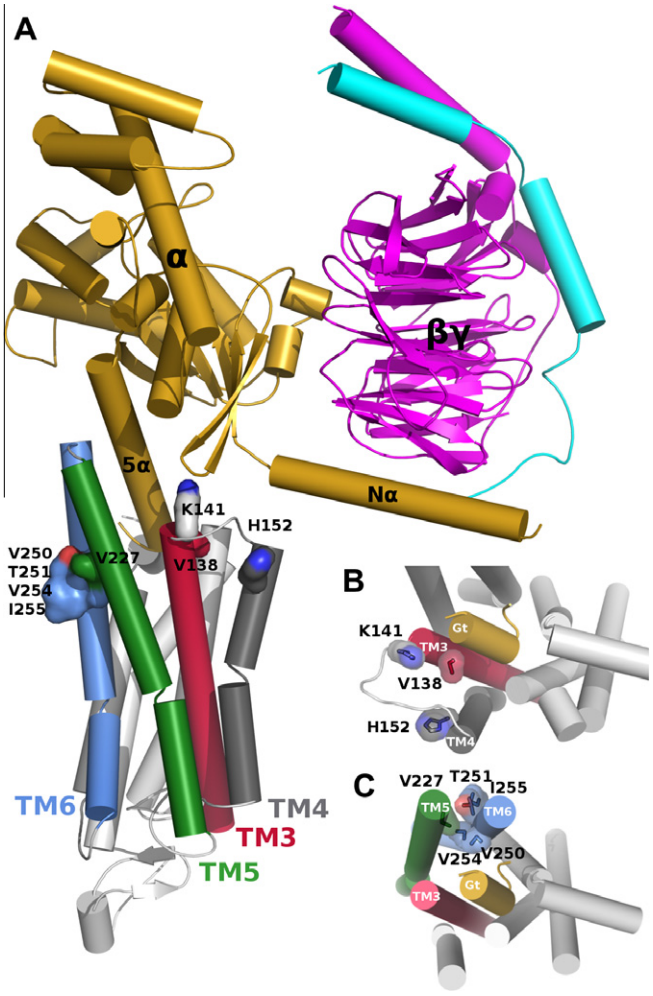

Fig. 3. Residues located at the TM3-C-II-TM4 and TM5-TM6 and their interaction with Gt. (A) Model of the opsin-Gt complex by superposition of 1GOT and 3DQB with helices displayed as cylinders. Opsin helices and loops are shown in white except TM3 in red, TM4 in grey, TM5 in green and TM6 in blue. For the G-protein subunits the color code is: Gtα (yellow), $G_t\beta$ (magenta), and $G_t\gamma$ (cyan). Mutated residues are highlighted with a van der Waals surface. (B) and (C) Models show in detail the two regions mutated in this study: TM3-C-II-TM4 and TM5-TM6, respectively. (For interpretation of the references to color in this figure legend, the reader is referred to the web version of this article.)

but interacts also with L226$^{5.61}$, V250 and V254 exhibit a large contact surface with residues L72$^{2.39}$ and L131$^{3.46}$, respectively; I255 contacts the functionally important Y223$^{5.58}$ and V227 does not interact directly with TM5. In the Gt-interacting opsin, all residues except V250 and V254 are facing out of the bundle and do not contact GtαCt. Thus, V227, T251 and V254 form a large surface of interaction between TMs 5 and 6. Importantly, V250 binds L344 and L349 of Gt via hydrophobic interactions (Gt residues are displayed in italics for clarity). These correspond to two fully conserved residues in all G-proteins, whereas V254 seems to be too short to contact Gt even though its side chain is facing inside.

Discussion

The rhodopsin mutants at the second and third cytoplasmic domains presented here, showed normal chromophore formation, no hydroxylamine sensitivity in the dark and photobleaching and acidification properties very similar to those of WT (Fig. 1, Table 2). None of the single mutants studied here showed dark state instability at 55 °C, but when these single mutants were combined (4CIII, 5CIII, 1CII-5CIII and 2CII-5CIII), their stability was dramatically reduced (Table 2). Regarding the active state, only the single K141R mutant exhibited a decreased stability, although without affecting its ability to activate Gt.

So, the results suggest that these mutants follow the same photoactivation cascade as the WT but the introduction of these mutations affects the helical packing and reduce the stability of the inactive state. With the exception of V138S, all C-II mutants exhibited a similar degree of Gt activation than the WT. V138 provides hydrophobic contacts at the junction of TM3 and loop C2, according to the recent crystal structure of opsin in its G-protein interacting conformation [28]. Additionally, it has previously been described that this amino acid, together with residues Y136, V137 and V139 would form a common important site for Gt interaction and/or activation [26]. We showed that V138S causes a 50% reduction in receptor functionality as a result of this motif perturbation. In a comparative study between rhodopsin and M2 muscarinic receptor C-II domain sequences, the related mutant V138C was found to markedly decrease the levels of Gt activation (75%) when V137 was simultaneously mutated to Phe. The effect was attributed to the different molar volumes of the two amino acids [36]. GtαCt exhibits two sides, a hydrophobic one that contacts the ends of TMs 5 and 6 and another, which contains polar and charged residues. V138 does not face the hydrophobic part, and consequently the effects of the V138S mutant are likely to be associated to the network of hydrogen bonds that connects the neighboring K141 with *E342, N343* and *E346* in GtαCt. Thus, the 2-fold decrease in activation for the mutant can be understood from the ability of S138 to interfere with such a network. This would be compatible with the lack of effect previously reported for the V138C mutant [55]. The reduced Gt activation shown by V138S could be reversed when it was conjugated with the K141R mutation. The increased volume of the Arg side-chain would compensate for the smaller Ser volume in creating an optimal site for Gt coupling. The combined mutant 3CII did not show the same effects as the single V138S mutant. So, even though the specific details are not fully understood, this behavior may be explained by the fact that both V138S and K141R mutants are affecting the network of interactions cited below.

Gt activation assay for C-III mutants showed an important reduction in receptor functionality. V227Y single mutant showed a 25% decrease of Gt activation, whereas the combined 4CIII mutant decreased up to a 75%. The crystal structure-based models suggest that activation observed for V227Y$^{5.62}$ would be caused by alterations at the interface between TMs 5 and 6. In particular, one possibility is that V227Y causes an alteration in K231$^{5.65}$, the counterpart of E247$^{6.30}$ in the active state, which is located one turn above [28]. Regarding 4CIII, the individual contributions of each amino acid is difficult to determine because the result would be influenced by the change in inter-helical interactions in both the inactive and active states as well as in their ability to interact with the G-protein. In a preceding study, the individual mutation of the four residues involved in 4CIII to Cys resulted in proteins that had a slightly larger activation (1.1–1.4 times) than the WT [55]. The crystal structures do not reveal a specific role for residue R252, a fact that, together with the present results, suggests that V250A and T251A are critical contributions to the 4CIII mutant behavior. Indeed, the crystal structure of opsin bound to GtαCt showed that V250 interacts with the two fully conserved Leu residues in the G-proteins, L344 and L349, a fact that is also supported by the presence of a hydrophobic residue at this position in 91% of human non-olfactory Class A GPCRs [56]. The lack of significant increase for Gi/qα activation, when compared to WT rhodopsin, for any of the mutants, indicates that the mutations introduced are not enough for changing the specificity for the G-protein. This is consistent with the previous finding that it is necessary to replace the complete second and third intracellular loops for partially changing the selectivity for the G-protein [42].

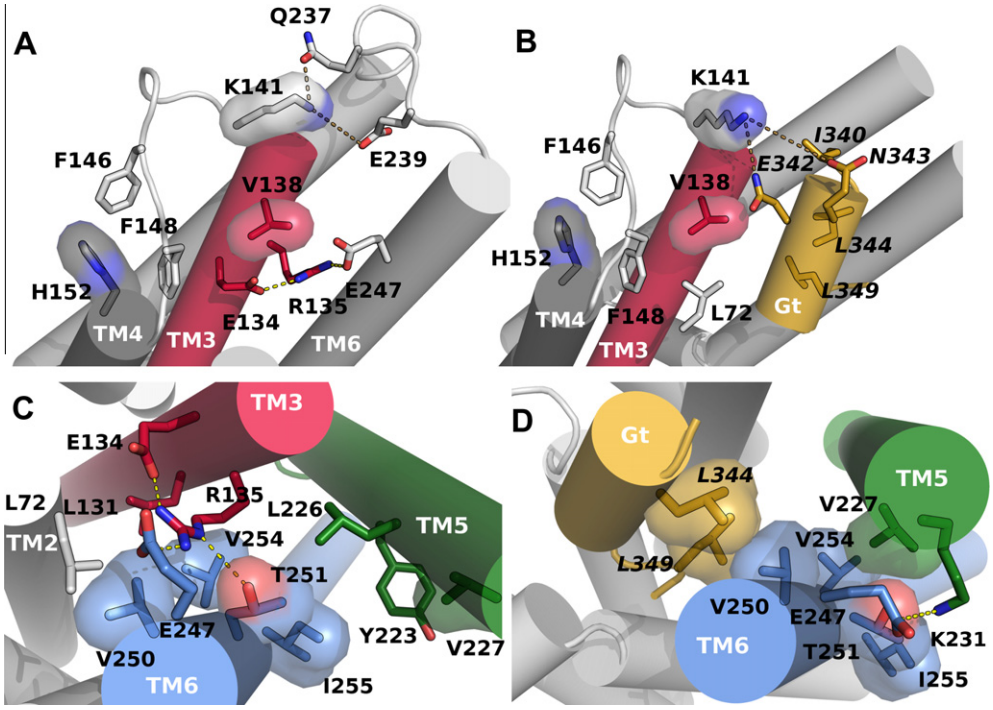

Fig. 4. Localization of the mutated residues in the crystal structures of inactive rhodopsin (panels A and C) and in the Gt-interacting opsin (panels B and D). Panels A and B show the C-II domain: V138$^{3.53}$, K141$^{3.56}$ and H152$^{4.41}$ and panels C and D the C-III domain: V227$^{5.62}$, V250$^{6.33}$, T251$^{6.34}$, V254$^{6.37}$ and I255$^{6.38}$. Helices are shown as light gray cylinders except: TM3 (red), TM4 (dark-grey), TM5 (green in panels C and B), TM6 (blue in panels C and D) and GtαCt (yellow). Mutated residues are shown as sticks and highlighted with a van der Waals surface. Dashed lines represent hydrogen bond interactions. All panels are views from the cytoplasmic side. (For interpretation of the references to color in this figure legend, the reader is referred to the web version of this article.)

Table 3
Summary of structural and sequence features of the single mutants used to construct the rhodopsin–M3 muscarinic mutants. From left to right: mutant name; numbering according to Ballesteros and Weinstein scheme [9]; main contact region of the residue in rhodopsin and in opsin; percentages of human class I GPCRs and (rod) opsins containing the original and the mutated residue; the preferred residue type at this position: hydrophobic: LIMPVAT, small: GSTCAV, bulky: LIM, H-bond: TSCHQNEDRK, aromatic: FHWY.

Mutant	B-W	Main contact in rhodopsin	Main contact in opsin		% Class I human	% (rod) opsins		% Class I human	% (rod) opsins	Pref. Type in Class I human
V138S	3.53	TM6	GαCt	V	7	88	S	14	1	Small: 83%
K141R	3.56	C-III loop	GαCt	K	9	78	R	13	11	H-bond: 74%
H152R	4.41	C-II loop	GαCt	H	7	57	R	24	8	H-bond: 62%, Hydrophobic: 31%
V227Y	5.62	TM6	TM6	V	8	38	Y	14	1	Hydrophobic: 51% (Bulky 32%), aromatic 31%
V250A	6.33	TM3	GαCt	V	16	70	A	33	0	Hydrophobic 84%
T251A	6.34	TM3	TM5	T	16	54	A	22	26	Hydrophobic 78%
V254L	6.37	TM3	TM5	V	23	67	L	36	1	Hydrophobic 93% (Bulky 60%)
I255S	6.38	TM5	-	I	7	36	S	5	0	Hydrophobic 67%

Regarding T251$^{6.34}$, additionally to being involved in the ionic-lock in the inactive state, it is also linked, in the active state, to the E247-K231 salt-bridge described above. The additive decrease of V227Y and 4CIII in the combined mutant is in agreement with the existence of two independent effects, which result in virtually no Gt activation. This finding suggests that V227, together with residues in TM6 (V250, T251, V254 and I255), forms a Gt recognition site and that the conjugation of these mutations completely alters the conformation of this interacting site resulting in a non-functional receptor. In the case of the combined mutations in C-II and C-III we observed that 1CII-5CIII mutant did not show any ability to activate Gt, whereas the addition of K141R (2CII-5CIII) modulated the rhodopsin–Gt interaction pattern in a way that partially restored the ability to activate the G protein, suggesting that K141R could be compensating by the mutations at the C-III cytoplasmic loop.

Conclusions

Overall, our results indicate that hydrophobic residues in TMs 3–6 of rhodopsin loops are involved in Gt activation by directly binding to the C-terminus or by modulating the interactions between TMs 3 and 6. We show that hydrophobic amino acids V138$^{3.53}$, V227, V250$^{6.33}$, V254$^{6.37}$ and I255$^{6.38}$ play a crucial role in Gt activation. These residues, which change their environment during the transition to the active state, form a Gt recognition site together with additional residues such as V137 and V139 [26]. These hydrophobic interactions play a critical role in efficient rhodopsin–Gt coupling and in modulating TMs movements. Similar kind of hydrophobic interactions, involving conserved hydrophobic residues [56], could also determine the specificity of other GPCR-G protein complexes, in addition to well established electrostatic interactions [49].

Acknowledgments

We thank Dr. L.J. del Valle for helpful discussions. This research was supported by grant from MICINN (SAF2008-04943-C02-02) to PG, UPC fellowship (fellowship from Universitat Politècnica de Catalunya to L.B. and D.T.), Fellowship from Ministerio de Educación y Ciencia (FPI to L.I. and M.A.) and contract grant from the Instituto de Salud Carlos III to A.C.

References

[1] P.A. Hargrave, Invest. Ophthalmol. Vis. Sci. 42 (2001) 3–9.
[2] T.P. Sakmar, S.T. Menon, E.P. Marin, E.S. Awad, Annu. Rev. Biophys. Biomol. Struct. 31 (2002) 443–484.
[3] J. Bockaert, J.P. Pin, EMBO J. 18 (1999) 1723–1729.
[4] J. Wess, FASEB J. 11 (1997) 346–354.
[5] M.J. Marinissen, J.S. Gutkind, Trends Pharmacol. Sci. 22 (2001) 368–376.
[6] K. Palczewski, T. Kumasaka, T. Hori, C.A. Behnke, H. Motoshima, B.A. Fox, I. Le Trong, D.C. Teller, T. Okada, R.E. Stenkamp, M. Yamamoto, M. Miyano, Science 289 (2000) 739–745.
[7] S.G. Rasmussen, H.J. Choi, D.M. Rosenbaum, T.S. Kobilka, F.S. Thian, P.C. Edwards, M. Burghammer, V.R. Ratnala, R. Sanishvili, R.F. Fischetti, G.F. Schertler, W.I. Weis, B.K. Kobilka, Nature 450 (2007) 383–387.
[8] T. Warne, M.J. Serrano-Vega, J.G. Baker, R. Moukhametzianov, P.C. Edwards, R. Henderson, A.G. Leslie, C.G. Tate, G.F. Schertler, Nature 454 (2008) 486–491.
[9] J.A. Ballesteros, H. Weinstein, Meth. Neurosci. 25 (1995) 366–428.
[10] R. Nygaard, T.M. Frimurer, B. Holst, M.M. Rosenkilde, T.W. Schwartz, Trends Pharmacol. Sci. 30 (2009) 249–259.
[11] E. Urizar, S. Claeysen, X. Deupi, C. Govaerts, S. Costagliola, G. Vassart, L. Pardo, J. Biol. Chem. 280 (2005) 17135–17141.
[12] V. Fodale, D. Quattrone, C. Trecroci, V. Caminiti, L.B. Santamaria, Br. J. Anaesth. 97 (2006) 445–452.
[13] M.A. Piggott, J. Owens, J. O'Brien, S. Colloby, J. Fenwick, D. Wyper, E. Jaros, M. Johnson, R.H. Perry, E.K. Perry, J. Chem. Neuroanat. 25 (2003) 161–173.
[14] S. Tucek, J. Jakubik, V. Dolezal, E.E. el-Fakahany, J. Physiol. Paris 92 (1998) 241–243.
[15] E.G. Peralta, A. Ashkenazi, J.W. Winslow, D.H. Smith, J. Ramachandran, D.J. Capon, EMBO J. 6 (1987) 3923–3929.
[16] A.P. Roszkowski, J. Pharmacol. Exp. Ther. 132 (1961) 156–170.
[17] R.B. Barlow, K.J. Berry, P.A. Glenton, N.M. Nilolaou, K.S. Soh, Br. J. Pharmacol. 58 (1976) 613–620.
[18] R. Hammer, C.P. Berrie, N.J. Birdsall, A.S. Burgen, E.C. Hulme, Nature 283 (1980) 90–92.
[19] T.I. Bonner, N.J. Buckley, A.C. Young, M.R. Brann, Science 237 (1987) 527–532.
[20] T.I. Bonner, A.C. Young, M.R. Brann, N.J. Buckley, Neuron 1 (1988) 403–410.
[21] J. Wess, Crit. Rev. Neurobiol. 10 (1996) 69–99.
[22] P.D. Garcia, R. Onrust, S.M. Bell, T.P. Sakmar, H.R. Bourne, EMBO J. 14 (1995) 4460–4469.
[23] H.E. Hamm, D. Deretic, A. Arendt, P.A. Hargrave, B. Koenig, K.P. Hofmann, Science 241 (1988) 832–835.
[24] R. Herrmann, M. Heck, P. Henklein, C. Kleuss, K.P. Hofmann, O.P. Ernst, J. Biol. Chem. 279 (2004) 24283–24290.
[25] T. Morizumi, H. Imai, Y. Shichida, J. Biochem. 134 (2003) 259–267.
[26] S. Acharya, Y. Saad, S.S. Karnik, J. Biol. Chem. 272 (1997) 6519–6524.
[27] J.H. Park, P. Scheerer, K.P. Hofmann, H.W. Choe, O.P. Ernst, Nature 454 (2008) 183–187.
[28] P. Scheerer, J.H. Park, P.W. Hildebrand, Y.J. Kim, N. Krauss, H.W. Choe, K.P. Hofmann, O.P. Ernst, Nature 455 (2008) 497–502.
[29] D.L. Farrens, C. Altenbach, K. Yang, W.L. Hubbell, H.G. Khorana, Science 274 (1996) 768–770.
[30] U. Gether, B.K. Kobilka, J. Biol. Chem. 273 (1998) 17979–17982.
[31] C. Altenbach, K. Yang, D.L. Farrens, Z.T. Farahbakhsh, H.G. Khorana, W.L. Hubbell, Biochemistry 35 (1996) 12470–12478.
[32] T.D. Dunham, D.L. Farrens, J. Biol. Chem. 274 (1999) 1683–1690.
[33] J. Klein-Seetharaman, E.V. Getmanova, M.C. Loewen, P.J. Reeves, H.G. Khorana, Proc. Natl. Acad. Sci. USA 96 (1999) 13744–13749.
[34] J.M. Janz, D.L. Farrens, J. Biol. Chem. 279 (2004) 29767–29773.
[35] S. Ye, E. Zaitseva, G. Caltabiano, G.F. Schertler, T.P. Sakmar, X. Deupi, R. Vogel, Nature 464 (2010) 1386–1389.
[36] T. Yamashita, A. Terakita, Y. Shichida, J. Biol. Chem. 275 (2000) 34272–34279.
[37] J. Hu, Y. Wang, X. Zhang, J.R. Lloyd, J.H. Li, J. Karpiak, S. Costanzi, J. Wess, Nat. Chem. Biol. 6 (2010) 541–548.
[38] E. Kostenis, B.R. Conklin, J. Wess, Biochemistry 36 (1997) 1487–1495.
[39] N. Blin, J. Yun, J. Wess, J. Biol. Chem. 270 (1995) 17741–17748.
[40] J. Liu, N. Blin, B.R. Conklin, J. Wess, J. Biol. Chem. 271 (1996) 6172–6178.
[41] F.Y. Zeng, A. Hopp, A. Soldner, J. Wess, J. Biol. Chem. 274 (1999) 16629–16640.
[42] J.M. Kim, J. Hwa, P. Garriga, P.J. Reeves, U.L. RajBhandary, H.G. Khorana, Biochemistry 44 (2005) 2284–2292.
[43] L. Ferretti, S.S. Karnik, H.G. Khorana, M. Nassal, D.D. Oprian, Proc. Natl. Acad. Sci. USA 83 (1986) 599–603.
[44] C.K. Meyer, M. Bohme, A. Ockenfels, W. Gartner, K.P. Hofmann, O.P. Ernst, J. Biol. Chem. 275 (2000) 19713–19718.
[45] R.S. Molday, D. MacKenzie, Biochemistry 22 (1983) 653–660.
[46] T. Sakamoto, H.G. Khorana, Proc. Natl. Acad. Sci. USA 92 (1995) 249–253.
[47] T.P. Sakmar, R.R. Franke, H.G. Khorana, Proc. Natl. Acad. Sci. USA 88 (1991) 3079–3083.
[48] I.I. Senin, L. Bosch, E. Ramon, E.Y. Zernii, J. Manyosa, P.P. Philippov, P. Garriga, Biochem. Biophys. Res. Commun. 349 (2006) 345–352.
[49] E. Ramon, A. Cordomi, L. Bosch, E.Y. Zernii, I.I. Senin, J. Manyosa, P.P. Philippov, J.J. Perez, P. Garriga, J. Biol. Chem. 282 (2007) 14272–14282.
[50] J. Li, P.C. Edwards, M. Burghammer, C. Villa, G.F. Schertler, J. Mol. Biol. 343 (2004) 1409–1438.
[51] The Pymol Molecular Graphics System, Version 1.2b5 DeLano Scientific, LLC.
[52] V. Hornak, R. Abel, A. Okur, B. Strockbine, A. Roitberg, C. Simmerling, Proteins 65 (2006) 712–725.
[53] S.P. Sheikh, T.A. Zvyaga, O. Lichtarge, T.P. Sakmar, H.R. Bourne, Nature 383 (1996) 347–350.
[54] B. Jastrzebska, Y. Tsybovsky, K. Palczewski, Biochem. J. 428 (2010) 1–10.
[55] K. Yang, D.L. Farrens, W.L. Hubbell, H.G. Khorana, Biochemistry 35 (1996) 12464–12469.
[56] B.K. Kobilka, X. Deupi, Trends Pharmacol. Sci. 28 (2007) 397–406.